Breathable core–shell microneedle patches for diabetic wound treatment

To cite this article: Lu Fan *et al* 2025 *Mater. Futures* **4** 025402

OPEN ACCESS
IOP Publishing | Songshan Lake Materials Laboratory

MATERIALS FUTURES

Mater. Futures 4 (2025) 025402 (10pp) https://doi.org/10.1088/2752-5724/adcbc6

Breathable core–shell microneedle patches for diabetic wound treatment

Lu Fan[1,2], Yu Wang[1], Li Wang[2], Xiang Lin[2], Xiaoju Wang[2], Luoran Shang[3,*], Hongbo Zhang[2,5,*] and Yuanjin Zhao[1,4,*]

[1] Department of Rheumatology and Immunology, Nanjing Drum Tower Hospital, School of Biological Science and Medical Engineering, Southeast University, Nanjing 210096, People's Republic of China
[2] Pharmaceutical Sciences Laboratory, Åbo Akademi University, Turku 20520, Finland
[3] Shanghai Xuhui Central Hospital, Zhongshan-Xuhui Hospital, and the Shanghai Key Laboratory of Medical Epigenetics, The International Co-laboratory of Medical Epigenetics and Metabolism (Ministry of Science and Technology), Institutes of Biomedical Sciences, Fudan University, Shanghai 200032, People's Republic of China
[4] Wenzhou Institute, University of Chinese Academy of Sciences, Wenzhou, Zhejiang 325001, People's Republic of China
[5] Turku Bioscience Centre, University of Turku and Åbo Akademi University, Turku 20520, Finland

E-mail: luoranshang@fudan.edu.cn, hongbo.zhang@abo.fi and yjzhao@seu.edu.cn

Received 3 January 2025, revised 25 March 2025
Accepted for publication 3 April 2025
Published 23 April 2025

Abstract

Microneedles have demonstrated valuable applications in diabetic wound management. Many endeavors are devoted to developing microneedles with well-designed structures and enhanced functions. Herein, we present an elaborate microneedle patch with breathability for wound healing by a multi-step replication method. The microneedle patch consists of a breathable porous supporting substrate and core–shell tips involving poly (vinyl alcohol) shells loaded with antimicrobial peptides (PVA@AMPs shell) and crosslinked Gelma cores encapsulated with exosomes (Gelma@exo core). The PVA was crosslinked with a ROS-responsive linker, which results in degradation of the microneedle shell in the inflammatory microenvironment, thus inducing the release of loaded AMPs to inhibit bacteria. Further, the exosomes continuously release from the exposed Gelma@exo core, promoting tissue regeneration and regulating the immune response. Besides, the high porosity of the supporting substrate makes the microneedle patches more suitable for chronic wounds. Based on these features, it was demonstrated that the microneedle patch exhibits desirable performance in *in vivo* animal tests. Thus, we believe that the proposed microneedle patches have remarkable potential in wound healing and related fields.

Supplementary material for this article is available online

Keywords: breathable, microneedle, hydrogel, exosome, diabetic wound

* Authors to whom any correspondence should be addressed.

1. Introduction

Diabetic ulcers (DU), a prevalent and serious complication associated with diabetes mellitus, is featured by chronic wound healing [1–5], which results in huge economic and health burdens worldwide [6, 7]. Numerous medical patches with natural or synthetic polymer compositions have been developed, showing immense value for the treatment of DU [8–11]. Especially, incorporating functional ingredients in patches can improve the therapeutic performances in wound repair [12–16]. For example, exosomes-encapsulated patches have demonstrated superior therapeutic effects owing to their distinctive immunoregulation and regeneration capacities [6, 17–19]. In addition, some antibacterial agents like antimicrobial peptides (AMPs), with the advantages of inhibiting microbial activity and preventing bacterial growth, are proven to be promising additives for medical patches for the antibacterial treatment of diabetic wounds [20–22]. Despite with many progresses, there is still room for improvement in terms of the structural design of the patch in order to control the spatial distribution of these functional ingredients and thus to improve the therapeutic efficacy [23–25]. Additionally, traditional blocky gel-based patches may fall short of the need for permeability [23, 26–28], which is unfavorable for chronic DU healing. Thus, developing novel patches with specific structural designs and high permeability for facilitating wound healing is still anticipated.

In this paper, we present an elaborate microneedle patch with free breathability for the treatment of diabetic wounds, as schemed in figure 1. Microneedles, known as minimal invasive transdermal devices, are important medical patches [29–32]. Particularly, core–shell microneedles, with a distinctive dual-layer architecture [33], offer appropriate control over spatial distributions of various functional materials encapsulated [34, 35]. Besides, porous materials have gained considerable attention due to their excellent gas permeability, providing a breathable environment conducive to wound healing [36–38]. Diverse strategies have been proposed for the construction of porous materials by using porogens as sacrificial substances including gas bubbles, solid particles, etc [39–41]. Therefore, we conceive that the integration of core–shell structured microneedles and porous materials can be expected to establish the elaborate, spatially distributed, and breathable microneedle patches.

Herein, we fabricated the desired core–shell structured microneedle patches with high permeability through a multi-step replication method. Such microneedle patch was comprised of core–shell tips and breathable backing. The tips consisted of poly (vinyl alcohol) shells loaded with antimicrobial peptides (PVA@AMPs shell), and Gelma cores encapsulating exosomes (Gelma@exo core). The breathable supporting substrate was a porous Gelma hydrogel layer prepared by using emulsified oil droplets as the porogen. The PVA hydrogel was crosslinked by mixing with a ROS-responsive linker N1-(4-boronobenzyl)-N3-(4-boronophenyl)-N1,N1,N3,N3-tetramethylpropane-1,3-diaminium (TSPBA), such that the microneedle shell can be triggered by ROS to gradually degrade, resulting in the release of loaded AMPs to inhibit bacteria growth. Meanwhile, exosomes were continuously released from the exposed Gelma@exo core, contributing to tissue regeneration and immunomodulation. Besides, benefitting from the high porosity and excellent breathability of the supporting substrate, the microneedle patch provided a well-ventilated environment, preventing exudate accumulation and reducing bacterial growth at the chronic wounds. Attributed to these features, it was demonstrated that such microneedle system exhibited promising performances in promoting collagen deposition, angiogenesis and anti-inflammation in a DU rat model. These results indicated that the proposed core–shell structured microneedle patches are promising for DU treatment and other relative disease therapy.

2. Methods

Materials: polyvinyl alcohol (PVA) and 2-hydroxy-2-methylpropiophenone (HMPP) were bought from Sigma-Aldrich. N1-(4-boronobenzyl)-N3-(4-boronophenyl)-N1,N1,N3,N3-tetramethylpropane-1,3-diaminium (TSPBA) was bought from Xi'an Qiyue Bio Tech Co., Ltd. Fluorescent nanoparticles were purchased from Thermo Fisher Scientific. Eumenitin was bought from Wuhan Haode Peptide Co., Ltd. *E. coli* and *S. aureus* were both obtained from BeNa Culture Collection. Deionized water was obtained by a Milli-Q Plus 185 water purification system.

Preparation of the breathable backing: a mixture of 20% Gelma and oil in a 1:1 ratio was emulsified using a homogenizer at 8000 rpm. Then, the emulsified solution was added to the backing of the core–shell microneedle mold and UV-cured. After solidification, the patch was demolded and immersed in alcohol for washing to remove the oil droplets. After totally cleaning, the patch was stored at 4 °C for later use.

Extraction of exosomes: firstly, mesenchymal stem cells (MSCs) were cultured in complete F12/DMEM medium. When the cell fusion degree approached 80%, we collected the cell supernatant. Then, exosomes were extracted using Quick Exovesicle Isolation Kit. The obtained exosomes were resuspended in PBS and stored at −80 °C for later use.

Fabrication of core–shell structured microneedle patches: a mixture of 3% PVA, TSPBA (2%), and AMPs was added to a microneedle PDMS mold. The solution was drawn into the needle cavities via vacuum; after overnight drying, the PVA shell layer formed. Subsequently, a mixture of 20% Gelma, 1% HMPP, and exosomes were added to the original mold. By centrifuging, the mixture solution filled the PVA shell cavities. Then, the excess liquid was gently removed, and a pre-prepared porous patch was applied. Subsequently, the whole microneedle patch was solidified by UV light. Finally, the core–shell microneedles with the breathable backing

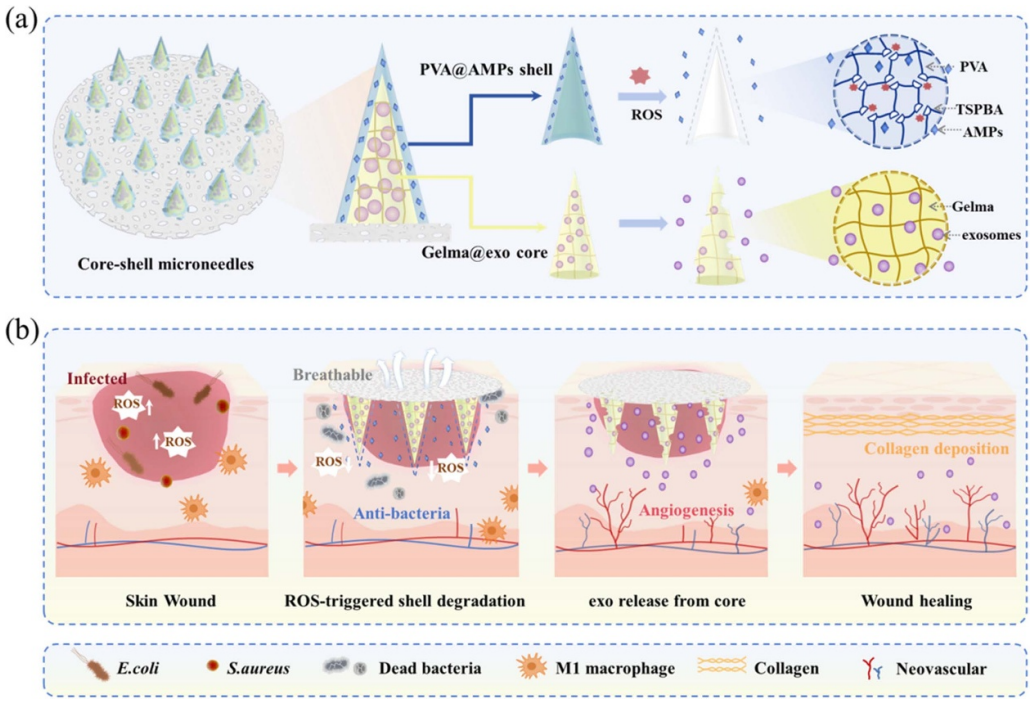

Figure 1. Schematic of the microneedle patch and its application on wound healing. (a) Core–shell structure of the microneedle patch. (b) The application of the microneedle patches for the treatment of diabetic wounds.

were carefully peeled off from the mold. We observed the obtained core–shell microneedles using an optical microscope (Olympus) and recorded the needle height and base diameter. Besides, the cross-sections of the microneedles and the porous backing were examined by a scanning electron microscope (SEM). Meanwhile, shell and core of the microneedles were labeled different colored fluorescent nanoparticles and observed under the fluorescence microscope.

Mechanical performance of core–shell microneedles: core–shell microneedles were placed tip-up on the platform of a mechanical strength testing machine (Instron, USA). The force sensor approached the microneedle tips at a speed of 0.2 mm s^{-1} and stopped after traveling 600 μm. The morphology of the core–shell microneedles before and after compression was recorded by an optical microscope.

PVA@TSPBA degradation and AMPs release behavior: PVA@TSPBA films loaded with RhB-labeled AMPs were prepared using the same mold. These films were then immersed in H_2O_2 (0, 0.1 mM and 0.5 mM) solutions. The morphology and degradation performance of the PVA@TSPBA films were imaged. At each time point, 100 μl of the above solutions were collected and fresh PBS (100 μl) were added. Finally, the collected solutions were assessed by optical density (OD) value.

Antibacterial assay: core–shell microneedles with a shell containing 60 μM AMPs were prepared. Subsequently, the blank core–shell microneedle (Microneedle) and the AMP-loaded core–shell microneedle (Microneedle@AMPs) were immersed in PBS with H_2O_2 (0.1 mM) solutions to obtain material leaching, respectively. After that, three groups were set up for the antibacterial experiment, including: Control group, the blank Microneedle leaching group, and the Microneedle@AMPs leaching group. *S. aureus* or *E. coli* suspension (10^8 CFU ml^{-1}) was added to each group and incubated at 37 °C. The bacterial viability in each group was then assessed using live/dead staining. Finally, bacterial suspensions from each group were diluted and plated on agar plates, and the formed colonies were recorded.

The exosomes release behaviour: firstly, 20% Gelma solution and 1 mg ml^{-1} red fluorescent nanoparticles were mixed and filled the PDMS mold, followed by UV curing and careful demolding. Then, the obtained Gelma microneedles were placed in PBS and shaking them at 37 °C and 100 rpm. At each time point, 100 μl of release solutions were collected and replaced with fresh PBS solutions. By measuring the fluorescence intensity, the release behavior of the nanoparticles was evaluated. At specific time, the images were captured after the Gelma microneedles were removed from the solution and dried at room temperature.

The degradation of Gelma microneedles: 20% Gelma solution was added to the mold, and then UV was used to solidify the solution, followed by careful demolding. Gelma microneedles were placed in PBS and shaking them at 37 °C and 100 rpm.

We measured the weight of freeze-dried Gelma microneedles at specific time points during 3 days.

The hemocompatibility experiment: fresh blood was centrifuged at 1500 rpm and then resuspended. Four groups mixed with the red blood cell solution were established: the deionized water group, the PBS group, the PVA@TSPBA group, and the Gelma group. The mixture samples were incubated at 37 °C for 2 h. Subsequently, the OD values of centrifuged supernatant in four groups were recorded. Meanwhile, the samples were photographed to observe the hemolysis.

The cytotoxicity experiment: firstly, the crosslinked PVA@TSPBA and Gelma patches were exposed to UV light overnight to complete sterilization. Then, they were co-cultured with NIH 3T3 cells, respectively. On days 1, 2, and 3 of co-culture, cell viability was confirmed by CCK-8 assay. Furthermore, live staining was performed for each group.

Scratch assay: human umbilical vein endothelial cells (HUVECs) (1×10^5) were seeded in a 24-well plate and cultured for 24 h. Subsequently, a scratch was made using the tip of a pipette and the wells were washed with PBS. Then, three groups were set up and co-cultured with the HUVECs: the control group, the blank Gelma microneedle leaching solution group, and the exosome-loaded Gelma microneedle leaching solution group. After 24 h, cell proliferation in each group were imaged. Meanwhile, the cell growth area during the 24 hour period was measured.

Tube formation assay: we set three groups: the control group, the blank Gelma microneedle leaching solution group, and the exosome-loaded Gelma microneedle leaching solution group. HUVECs (2×10^4) were seeded in a 48-well plate and co-cultured with three groups, respectively. After 4 h culture, cells in each group was stained with calcein-AM and imaged.

Macrophage polarization assays: three groups were set and co-cultured with RAW264.7 cells: the Control group, the LPS group, and the LPS + exosome-loaded Gelma microneedle group. RAW264.7 cells were cultured in DMEM medium in the control group. For the other two groups, 200 ng ml^{-1} LPS was added. After 6 h, the cells in the LPS + exosome-loaded microneedle group were co-cultured with the leachate from Gelma microneedles loaded with exosomes. After 24 h, the cells in each group were stained with anti-CD86 for flow cytometry.

In vivo *wound healing experiment*: to establish a type 1 diabetes model, rats were intraperitoneally injected by streptozotocined (STZ, 50 mg kg^{-1} rat body weight) until the blood glucose exceeded 16.7 mmol l^{-1}. After that, circular full-thickness wounds were created on the rats' back skin, followed by bacterial suspension injection into wounds. Five groups of rats were randomly divided and treated with PBS (Control), blank microneedle patches (G I: MNs), microneedle patches with AMPs loaded in the shell (G II: MNs@AMPs), microneedle patches with exosomes loaded in the core (G III: MNs@exo), as well as microneedle patches with AMPs loaded in the shell and exosomes loaded in the core (G IV: MNs@AMPs@exo). During treatment, 3M tapes were used to fix the edges of patch to rats' back. Wounds were imaged on day 0, 2, 6, 10, and 12 of treatment. Meanwhile, wound areas were assessed. During observation, the patch was removed to better observe and record the wound states. On the 12th day, all rats were euthanized, and wound tissues were collected for further analysis, including IL-6 staining, hematoxylin and eosin (H&E) staining, Mason staining, CD31 staining and HIF-1α staining.

3. Results and discussion

In a typical experiment, the core–shell structured microneedle patches were fabricated by a multi-step replication method (figure 2(a)). Briefly, an aqueous solution of poly (vinyl alcohol) (PVA) was mixed with TSPBA and Eumenitin-a kind of antimicrobial peptide (AMP), and was totally filled in the cavities of a PDMS mold. After drying overnight, a thin PVA cross-linked layer was formed at the inner wall of the mold. The porous supporting substrate was composed of Gelma and fabricated by photo-crosslinking, with oil droplets, formed through emulsification, serving as the porogen. The substrate was then stored at 4 °C for use in the following steps. After that, a Gelma solution with exosomes was stuffed to the cavities of the mold. Then, the extra solution was removed, and the pre-prepared porous substrate was applied. Subsequently, the whole system went thought UV solidification and demolding to obtain the microneedle patch. The resultant microneedle patch showed an excellent morphology with conical tips orderly arranged on the backing substrate (figure 2(b)). The measured height and diameter of the circular base of the needle were shown in figures 2(c) and (d), which demonstrated the relatively uniform size of the microneedles.

Subsequently, the core–shell structure of microneedles was characterized by a fluorescence microscope (figures 2(e)–(g)). The PVA shell and Gelma core was loaded with red and green fluorescent nanoparticles, respectively. The images showed the distinct shell and core architecture of the microneedles. To further confirm such structure, SEM was utilized to characterize the cross-section view of microneedles (figure 2(h)), which exhibited a clear double-layer structure. Besides, the exosomes exhibit a cup-shaped vesicular structure with a particle size of approximately 130 nm (figure S1). To prove the porous structure of the patches, SEM was utilized to characterize the supporting substrate of the microneedles (figures 2(i) and S2). Results displayed that numerous pores were distributed on the patch compared with the pure Gelma patch, indicating the high porosity of the supporting substrate, which is favorable for wound breathability. Besides, the penetration to skin is an important indicator for evaluating microneedles. The tolerable compressive force of the core–shell microneedles

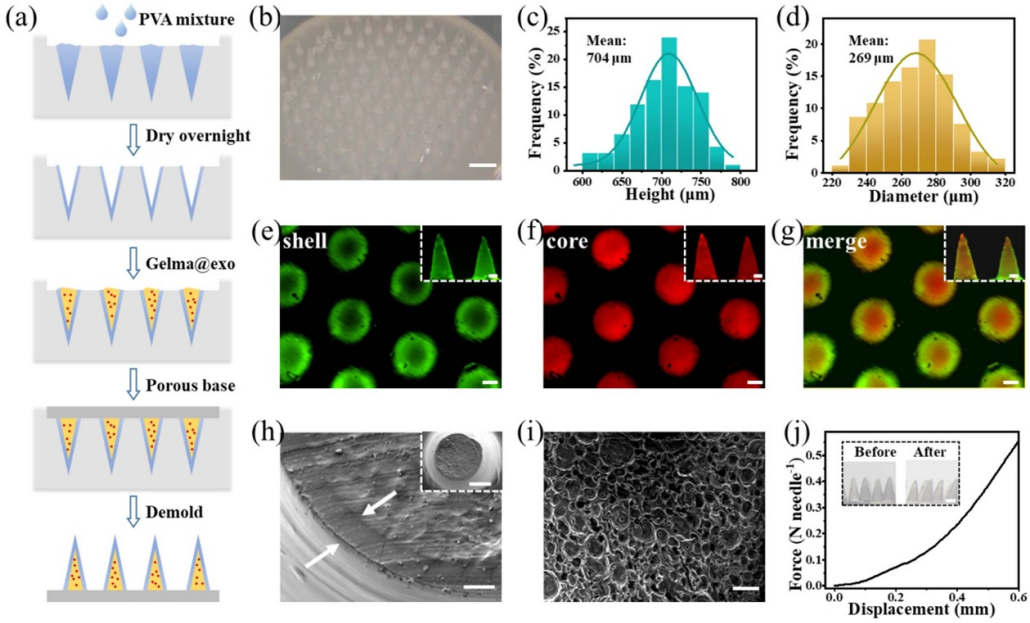

Figure 2. (a) Illustration of the fabrication process of the core–shell microneedles. (b) Optical image of the core–shell microneedles. Scale bars: 0.8 mm. (c), (d) (c) Tip height and (d) base diameter of the core–shell microneedles. (e)–(g) Fluorescent images of (e) PVA shell (green), (f) Gelma core (red), and (g) merged. All scale bars: 100 μm. (h) SEM images of the cross-section of the core–shell structured microneedles. Scale bars are 10 μm in (h) and 50 μm in the inset. (i) SEM image of the backing substrate of the porous patch. Scale bars: 200 μm. (j) The compressive force–displacement curve of the core–shell microneedles. Scale bar of the inset: 200 μm.

was measured as around 0.5 N per needle (figure 2(j)). The microneedles pressed on the rat's skin left an insert mark, indicating the ability to penetrate the skin (figure S3).

After that, we tested the degradation profile of the PVA shell and the antibacterial activity of core–shell microneedles. Infected chronic wounds are accompanied by elevated ROS levels. Compared to non-responsive microneedles, ROS-responsive microneedles are designed to actively trigger drug release in response to ROS, enabling on-demand release of AMPs. The core–shell structured microneedles were immersed in a H_2O_2 solution simulating the microenvironment of infected diabetic wounds. This results in gradual degradation of the PVA shell due to the existence of the ROS-responsive TSPBA, and consequently, the loaded AMPs can be gradually released (figure 3(a)). Hydrogel films made up of PVA and TSPBA (PVA@TSPBA films) were prepared. It was found that these films performed different degradation state in PBS, 0.1 mM and 0.5 mM H_2O_2 solutions (figure 3(b)). After 24 h, PVA@TSPBA films degraded almost completely in H_2O_2 solutions and more rapidly with increased H_2O_2 concentration, while it exhibited no significant change in PBS. Furthermore, the cumulative release of AMPs was measured during the process (figure 3(c)). It was observed that within 24 h, approximately 76.54% of the loaded AMPs was released in a 0.1 mM H_2O_2 solution.

Then, we further verified the *in vitro* antibacterial activity. AMPs solutions with different concentrations were co-cultured with bacteria (figures S4 and S5). Considering the effective antimicrobial activity and that the AMPs are gradually released from the shell of the microneedles, 60 μM AMPs was chosen for the following experiments. Then, blank core–shell microneedles (Microneedles) leaching and core–shell microneedles loaded with AMPs (Microneedles@AMPs) leaching were cultured with *E. coli* or *S. aureus*, respectively. Bacterial live/dead staining results indicated that Microneedles@AMPs group had superior antibacterial properties than control and blank microneedles groups (figure 3(e)). According to the statistics of the bacterial viability, it was manifested that the AMPs-loaded microneedles group killed the greatest number of *E. coli* and *S. aureus* (figure 3(d)). Additionally, the Microneedles@AMPs group also exhibited the least bacterial colonies than other groups (figure 3(f)). Collectively, the AMPs-loaded core–shell microneedles could remarkably inhibit bacteria owing to the ROS-triggered degradation of the PVA shell and the release of the loaded AMPs.

MSC-derived exosomes have been demonstrated with therapeutic values in chronic wounds, due to their superb angiogenesis and anti-inflammatory bioactivities [29]. To investigate the release behavior of exosomes, we performed qualitative and quantitative analyses of exosome release and several cellular experiments. Red fluorescent nanoparticles (size: 100 nm) were encapsulated in Gelma microneedles as a model of the exosomes because of the similar particle size, and the microneedles were then immersed in PBS. We recorded the fluorescence intensity at specific time (figures 4(a) and (b)). Results showed that the nanoparticle release was rapid in the first 12 h, reaching about 38.68% of total amount. Over the next 4 d, the release gradually slowed, and reached a plateau value around 80.43%. This result was consistent with the

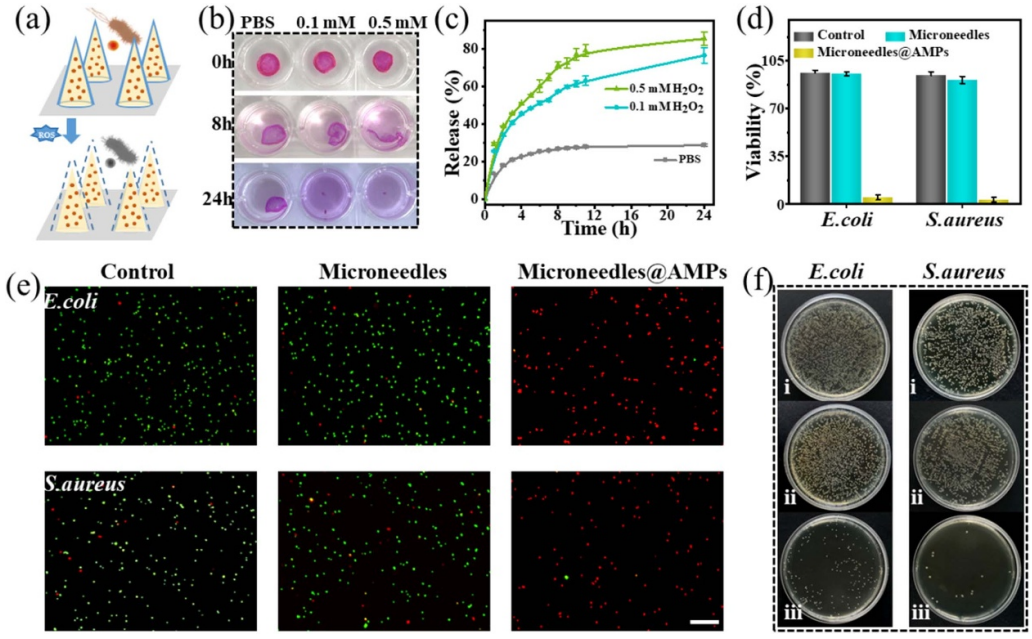

Figure 3. (a) Illustration of the antibacterial process of the core–shell microneedles. (b) Degradation state of PVA@TSPBA films in different concentrations of H_2O_2 solutions. (c) Cumulative release profile of AMPs from PVA@TSPBA films. (d), (e) The antibacterial effects of different microneedles. Scale bars: 50 mm. (f) Images of bacterial colonies on the culture plate in (i) control, (ii) microneedles and (iii) microneedles@AMPs groups.

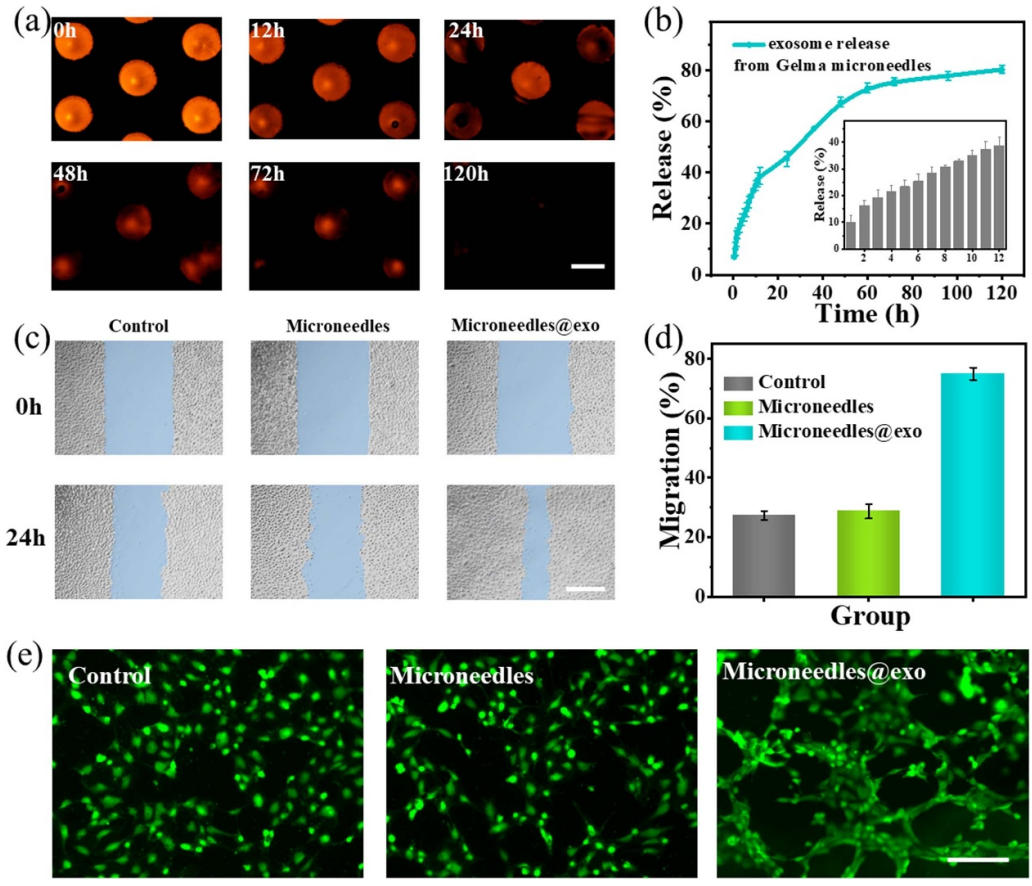

Figure 4. (a) Fluorescence images of Gelma microneedle loaded with red fluorescent nanoparticles at specific time points. (b) Cumulative release of the fluorescence nanoparticles from Gelma microneedles. (c) Scratch test results between different groups for 0 and 24 h. (d) Quantitative statistics of cell migration area within 12 h. (e) Tube formation in different groups. All scale bar: 200 μm.

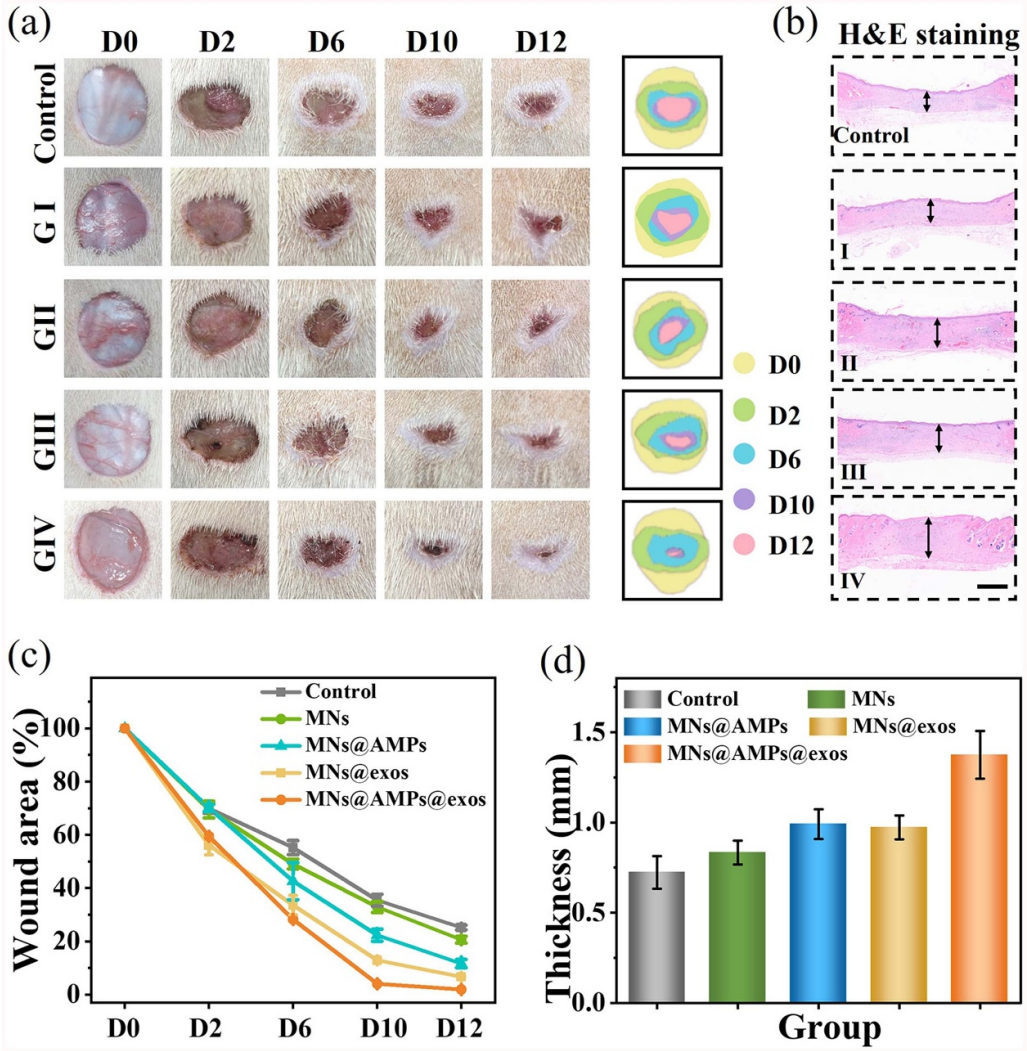

Figure 5. (a) Wound recovery in different groups and the contour of the wound surface. (G I: MNs, G II: MNs@AMPs, MNs@exo, G IV: MNs@AMPs@exo). (b) H&E staining of wounds in different groups on day 12. Scale bars: 1 mm. (c) Statistics of wound area in different days and groups. (d) Dermis thickness of wounds in different groups.

degradation performance of the Gelma microneedles (figure S6). To evaluate the suitability of core–shell microneedles for co-culture with cells and subsequent *in vivo* therapeutic applications, we conducted cytocompatibility and hemolysis assays (figures S7 and S8). Results displayed that neither needle tip nor backing material had significant impact on the cell proliferation, and both materials exhibited low hemolysis rates, indicating the satisfactory cytocompatibility and good hemocompatibility

To verify the ability of the encapsulated exosomes in promoting cell proliferation, HUVECs were cultured with the leaching liquor of blank Gelma microneedles (Microneedle) and exsomes loaded Gelma microneedles (Microneedle@exo). Scratch assay results revealed that the cells in the Microneedle@exo group showed faster scratch closure within 24 h (figure 4(c)). Quantitative analysis of cell migration in each group also showed that the cells co-cultured with the leaching liquor of Microneedle@exo achieved 74.96% migration, significantly higher than the other two groups (figure 4(d)). Besides, angiogenesis acts a viral role for wound healing. To confirm the angiogenic ability of these exosomes, we conducted a tube formation experiment (figures 4(e) and S9). It was displayed that HUVECs in Microneedle@exo group have more tube structures compared to control and blank Microneedles groups, indicating the effectively effects for angiogenesis. In addition, exosomes from Gelma microneedles efficiently reduced the proinflammatory M1 macrophages (figure S10), beneficial for alleviating inflammation in diabetic wounds.

To evaluate the *in vivo* therapeutic effects of core–shell microneedles, a diabetic infected wound model was established and then received different treatments. In brief, the diabetes rat model was established by STZ injection, followed by excising circular wounds with a diameter of 1 cm on backs (figure S11). After application of a bacterial solution to the wound area, rats were randomly divided into five groups according to various treatment including PBS (Control), blank microneedle patches (G I: MNs), microneedle patches with

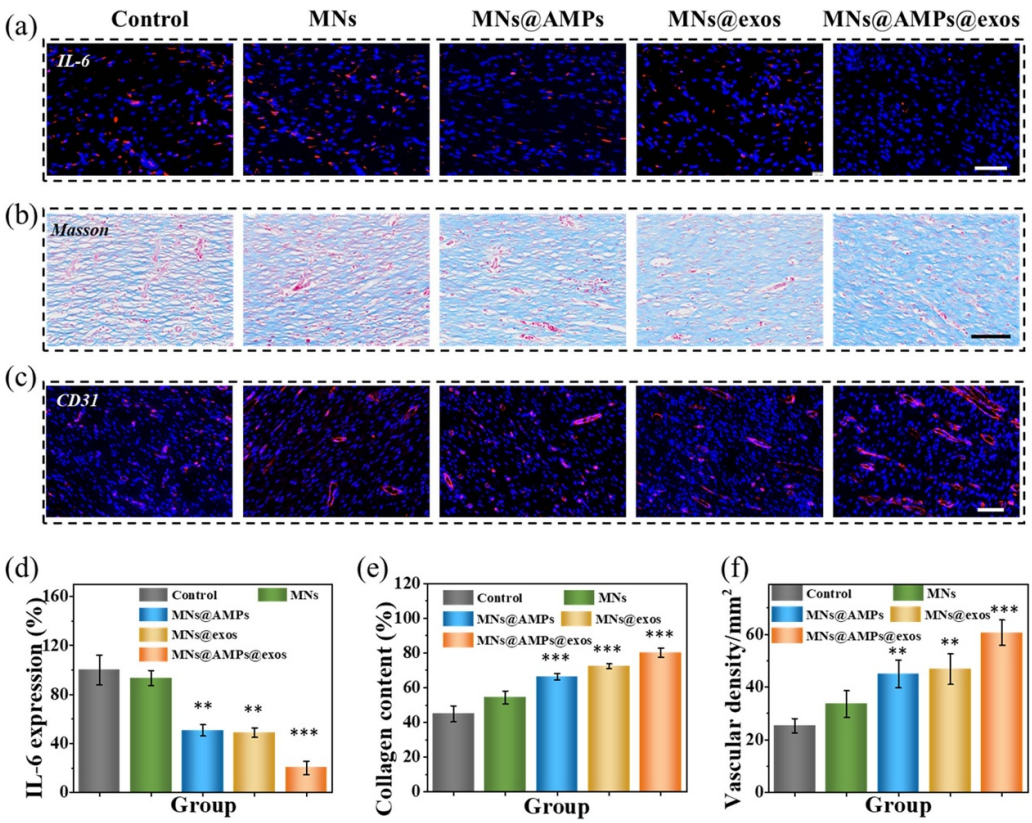

Figure 6. (a)–(c) (a) IL-6, (b) Masson staining, and (c) immunofluorescence staining of CD31 in different groups of rats wound beds on day 12. (d)–(f) (d) Quantitative analysis of IL-6 expression, (e) collage deposition, and (f) vascular density in different groups. (* indicates $P < 0.05$, ** indicates $P < 0.01$, and *** indicates $P < 0.001$). Scale bar in (a): 50 μm. Scale bars in (b) and (c): 100 μm.

AMPs loaded in the shell (G II: MNs@AMPs), microneedle patches with exosomes loaded in the core (G III: MNs@exo), as well as microneedle patches with AMPs loaded in the shell and exosomes loaded in the core (G IV: MNs@AMPs@exo). The photos of the diabetic wounds were recorded and quantitative analysis of wound area was assessed at specific time points in 12 d (figures 5(a) and (c)). The wounds recovery in G II and G III were both better than G I and Control, indicating the effect of AMPs and exosomes. In comparison, the G IV presented the best therapeutic effect and the smallest remaining wound area, owing to the co-delivery of AMPs and exosomes from the core–shell microneedle patches. Furthermore, we conducted the H&E staining on rat wounds and quantitative analysis of granulation tissue (figures 5(b) and (d)). G IV displayed the thickest granulation tissue, confirming improved tissue regeneration and healing ability.

To investigate the biological mechanism of the healing process, interleukin-6 (IL-6) staining, Masson staining, and CD31 immunofluorescent staining were performed. IL-6 staining was selected to evaluate the inflammatory stage during the healing process. Given the antibacterial properties of AMPs and the anti-inflammatory properties of exosomes, G II, G III, and G IV all exhibited reduced IL-6 expression compared with Control and G I (figures 6(a) and (d)). Furthermore, IL-6 mRNA expression was also detected by qRT-PCR assay (figure S12). Among them, G IV had the lowest IL-6 expression, which can be attributed to the combined effects of AMPs and exosomes. Collagen deposition represents another important index in wound healing, which was detected by Masson staining. Qualitative and quantitative results of Masson staining together proved that wound tissue of G IV had more collagen fiber formed and arranged, indicating the better tissue regeneration performance (figures 6(b) and (e)). Remarkably, angiogenesis is a vital step for wound recovery, which was evaluated by immunofluorescent staining of CD31 (figure 6(c)). Wound tissue of G IV revealed the most effective new blood vascular formation and density, due to the pro-angiogenic ability of exosomes. Quantitative analysis further demonstrated enhanced capacity for angiogenesis of G IV, as shown in figure 6(f). Finally, we performed HIF-1α staining to assess the hypoxic condition of the tissue. The results indicated that compared to the control group, the hypoxia in the wound area of the G IV group was alleviated, possibly due to the combined effect of the breathable basement and therapeutic active factors (figure S13). Collectively, it can be concluded that the MNs@AMPs@exo patches own remarkable potential for wound healing by reducing inflammation, facilitating collagen deposition, and promoting angiogenesis.

4. Conclusion

In summary, we have proposed a breathable core–shell structured microneedle patch for enhanced diabetic wound healing. The microneedle patch was composed of core–shell tips and breathable backing. The tips consisted of PVA@AMPs shell and Gelma@exo core. Meanwhile, the breathable supporting substrate possessed numerous pores that was conducive to breathability. Given the ROS-responsive linker TSPBA in the PVA hydrogel, the microneedle shell can be gradually degraded, resulting in the release of loaded AMPs, which was further beneficial to inhibit bacteria growth. Subsequently, exosomes can be continuously released from the exposed Gelma@exo core. *In vitro* results have proved the excellent effects of the microneedles in promoting fibroblasts migration and angiogenesis, as well as suppressing M1-type macrophages. Benefiting from these, animal experiments have demonstrated that such microneedle patch exhibited practical values in collagen deposition, angiogenesis, and anti-inflammation in a rat model.

5. Future perspective

The proposed breathable core–shell microneedle patches have promising prospects for various wound treatment and other relative biomedical applications. For instance, the core–shell structure of microneedles allows for the spatial and temporal loading of different therapeutic components, aiming at stage-specific treatment of wounds. Among them, the ROS-responsive shell facilitates the on-demand release of AMPs, thereby preventing excessive drug accumulation. However, in animal applications, the concentration of ROS at wound sites is not constant and controllable. It will lead to an incompletely degraded ROS-responsive shell, hindering the release efficiency of exosomes encapsulated within the microneedle core. In future, we will investigate how ROS with varying concentrations influences drug release behaviors from the core microneedles covered by shell, in order to better explore the impact of ROS levels on the release behavior of core-encapsulated therapeutics in practical application. In addition, to visually monitor the ROS levels at the wound site, ROS-responsive materials inducing luminescence or color changes, such as polydiacetylene and 3,3', 5,5'—tetramethylbenzidine, can be designed and introduced into microneedle patches. With these improvements, it is expected to greatly advance the application potential of core–shell microneedles, paving the way for wound treatment in clinic.

Acknowledgment

This work is funded by Research Project (347897), Solution for Health Profile (336355), InFLAMES Flagship (337531) Grants and Printed Intelligence Infrastructure (PII-FIRI) from Research Council of Finland. This study is part of the activities of the Åbo Akademi University Foundation (SÅA) funded Center of Excellence in Research "Materials-driven solutions for combating antimicrobial resistance (MADNESS).

Ethical statement

All animal experiments were approved by the Animal Investigation Ethics Committee of Wenzhou Institute of University of Chinese Academy of Sciences (No. WIUCAS23082401).

Conflict of interest

The authors declare no competing financial interests.

Author contributions

Y.J.Z., H.B.Z. and L.R.S. conceived the idea and designed experiments. L.F. conducted experiments and wrote the manuscript. Y.W. assisted in discussion and paper writing. L.W. assisted in animal experiments. L.W., X.L. and X.J.W. revised the manuscript and checked the grammar.

ORCID iDs

Lu Fan https://orcid.org/0009-0004-2553-8525
Hongbo Zhang https://orcid.org/0000-0002-1071-4416

References

[1] Wang C, Shirzaei Sani E, Shih C-D, Lim C T, Wang J, Armstrong D G and Gao W 2024 Wound management materials and technologies from bench to bedside and beyond *Nat. Rev. Mater.* **9** 550–66
[2] Theocharidis G *et al* 2022 A strain-programmed patch for the healing of diabetic wounds *Nat. Biomed. Eng.* **6** 1118–33
[3] Falanga V, Isseroff R R, Soulika A M, Romanelli M, Margolis D, Kapp S, Granick M and Harding K 2022 Chronic wounds *Nat. Rev. Dis. Primers* **8** 50
[4] Kavanagh F, Rozen W, Seth I and Cuomo R 2024 Exploring the efficacy of negative pressure wound therapy in the management of mycobacterium ulcerans wounds: a comprehensive literature review *Plast. Aesthet. Res.* **11** 43
[5] Pignet A-L, Hecker A, Voljc T, Carnieletto M, Watzinger N and Kamolz L-P 2024 The use of acellular fish skin grafts in burns and complex trauma wounds: a systematic review of clinical data *Plast. Aesthet. Res.* **11** 40
[6] Han X, Saengow C, Ju L, Ren W, Ewoldt R H and Irudayaraj J 2024 Exosome-coated oxygen nanobubble-laden hydrogel augments intracellular delivery of exosomes for enhanced wound healing *Nat. Commun.* **15** 3435
[7] Gravitz L 2018 Skin *Nature* **563** S83
[8] Zhi Y, Che J, Zhu H, Liu R and Zhao Y 2023 Glycyrrhetinic acid liposomes encapsulated microcapsules from microfluidic electrospray for inflammatory wound healing *Adv. Funct. Mater.* **33** 2304353
[9] Ding X, Yu Y, Li W and Zhao Y 2023 *In situ* 3D-bioprinting MoS_2 accelerated gelling hydrogel scaffold for promoting chronic diabetic wound healing *Matter* **6** 1000–14
[10] Fu X, Wang J, Qian D, Xi L, Chen L, Du Y, Cui W and Wang Y 2023 Oxygen atom-concentrating short fibrous sponge regulates cellular respiration for wound healing *Adv. Fiber Mater.* **5** 1773–87
[11] Fu X, Wang J, Qian D, Chen Z, Chen L, Cui W and Wang Y 2023 Living electrospun short fibrous sponge via engineered nanofat for wound healing *Adv. Fiber Mater.* **5** 979–93

[12] Yao X, Zhu G, Zhu P, Ma J, Chen W, Liu Z and Kong T 2020 Omniphobic ZIF-8@hydrogel membrane by microfluidic-emulsion-templating method for wound healing *Adv. Funct. Mater.* **30** 1909389
[13] Hu S *et al* 2023 An all-in-one "4A hydrogel": through first-aid hemostatic, antibacterial, antioxidant, and angiogenic to promoting infected wound healing *Small* **19** 2207437
[14] Li H, Cheng F, Wei X, Yi X, Tang S, Wang Z, Zhang Y S, He J and Huang Y 2021 Injectable, self-healing, antibacterial, and hemostatic N,O-carboxymethyl chitosan/oxidized chondroitin sulfate composite hydrogel for wound dressing *Mater. Sci. Eng.* C **118** 111324
[15] Cheng H, Shi Z, Yue K, Huang X, Xu Y, Gao C, Yao Z, Zhang Y S and Wang J 2021 Sprayable hydrogel dressing accelerates wound healing with combined reactive oxygen species-scavenging and antibacterial abilities *Acta Biomater.* **124** 219–32
[16] Wang L, Ding X, Fan L, Filppula A M, Li Q, Zhang H, Zhao Y and Shang L 2024 Self-healing dynamic hydrogel microparticles with structural color for wound management *Nano-Micro Lett.* **16** 232
[17] Song Y *et al* 2023 Adipose-derived mesenchymal stem cell-derived exosomes biopotentiated extracellular matrix hydrogels accelerate diabetic wound healing and skin regeneration *Adv. Sci.* **10** 2304023
[18] Gan J, Zhang X, Ma W, Zhao Y and Sun L 2022 Antibacterial, adhesive, and MSC exosomes encapsulated microneedles with spatio-temporal variation functions for diabetic wound healing *Nano Today* **47** 101630
[19] Li M, Fang F, Sun M, Zhang Y, Hu M and Zhang J 2022 Extracellular vesicles as bioactive nanotherapeutics: an emerging paradigm for regenerative medicine *Theranostics* **12** 4879–903
[20] Konno K *et al* 2006 Eumenitin, a novel antimicrobial peptide from the venom of the solitary eumenine wasp Eumenes rubronotatus *Peptides* **27** 2624–31
[21] Li Y, Saiding Q, Wang Z and Cui W 2024 Engineered biomimetic hydrogels for organoids *Prog. Mater. Sci.* **141** 101216
[22] Geng X, Zhang N, Li Z, Zhao M, Zhang H and Li J 2024 Iron-doped nanozymes with spontaneous peroxidase-mimic activity as a promising antibacterial therapy for bacterial keratitis *Smart Med.* **3** e20240004
[23] Zhang S, Qi C, Zhang W, Zhou H, Wu N, Yang M, Meng S, Liu Z and Kong T 2023 *In situ* endothelialization of free-form 3D network of interconnected tubular channels via interfacial coacervation by aqueous-in-aqueous embedded bioprinting *Adv. Mater.* **35** 2209263
[24] Zhang Y *et al* 2023 Scarless wound healing programmed by core-shell microneedles *Nat. Commun.* **14** 3431
[25] Lin X, Fan L, Wang L, Filppula A M, Yu Y and Zhang H 2023 Fabricating biomimetic materials with ice-templating for biomedical applications *Smart Med.* **2** e20230017
[26] Liu Z, Wan X, Wang Z L and Li L 2021 Electroactive biomaterials and systems for cell fate determination and tissue regeneration: design and applications *Adv. Mater.* **33** 2007429
[27] Mirhaj M, Labbaf S, Tavakoli M and Seifalian A M 2022 Emerging treatment strategies in wound care *Int. Wound J.* **19** 1934–54
[28] Chen Z, Lv Z, Zhuang Y, Saiding Q, Yang W, Xiong W, Zhang Z, Chen H, Cui W and Zhang Y 2023 Mechanical signal-tailored hydrogel microspheres recruit and train stem cells for precise differentiation *Adv. Mater.* **35** 2300180
[29] Zhang X, Gan J, Fan L, Luo Z and Zhao Y 2023 Bioinspired adaptable indwelling microneedles for treatment of diabetic ulcers *Adv. Mater.* **35** 2210903
[30] Chang H *et al* 2021 Cryomicroneedles for transdermal cell delivery *Nat. Biomed. Eng.* **5** 1008–18
[31] Fan L, Zhang X, Nie M, Xu Y, Wang Y, Shang L, Zhao Y and Zhao Y 2022 Photothermal responsive microspheres-triggered separable microneedles for versatile drug delivery *Adv. Funct. Mater.* **32** 2110746
[32] Kusama S, Sato K, Matsui Y, Kimura N, Abe H, Yoshida S and Nishizawa M 2021 Transdermal electroosmotic flow generated by a porous microneedle array patch *Nat. Commun.* **12** 658
[33] Zhang W, Cai L, Gan J and Zhao Y 2024 Photothermal responsive porous hollow microneedles as Chinese medicine versatile delivery system for wound healing *Smart Med.* **3** e20240007
[34] Yang H, Jiang X, Zeng Y, Zhang W, Yuan Q, Yin M, Wu G and Li W 2023 A swellable bilateral microneedle patch with core-shell structure for rapid lactate analysis and early melanoma diagnosis *Chem. Eng. J.* **455** 140730
[35] Lyu S *et al* 2024 A differential-targeting core–shell microneedle patch with coordinated and prolonged release of mangiferin and MSC-derived exosomes for scarless skin regeneration *Mater. Horiz.* **11** 2667–84
[36] Zhang W, Jing H, Niu Q, Wu Z, Sun Y, Duan Y and Wang X 2024 Sprayable, thermosensitive hydrogels for promoting wound healing based on hollow, porous and pH-sensitive ZnO microspheres *J. Mater. Chem.* B **12** 7519–31
[37] Lin Z, Xie W, Cui Z, Huang J, Cao H and Li Y 2023 3D printed alginate/gelatin-based porous hydrogel scaffolds to improve diabetic wound healing *Giant* **16** 100185
[38] Tang L, Guo Z, Zhao Q, Fan X, Pu Y, He B and Chen J 2024 A biodegradable Janus sponge for negative pressure wound therapy *Biomacromolecules* **25** 2542–53
[39] Kankala R K, Zhao J, Liu C, Song X, Yang D, Zhu K, Wang S, Zhang Y S and Chen A 2019 Highly porous microcarriers for minimally invasive *in situ* skeletal muscle cell delivery *Small* **15** 1901397
[40] Fan L, Zhang X, Wang L, Song Y, Yi K, Wang X, Zhang H, Li L and Zhao Y 2024 Bio-inspired porous microneedles dwelled stem cells for diabetic wound treatment *Adv. Funct. Mater.* **34** 2316742
[41] Zhuang P *et al* 2024 In situ generating CO gas for destroying bacterial biofilms *Nano Today* **56** 102296